IEEE Access
Multidisciplinary | Rapid Review | Open Access Journal

Received June 11, 2019, accepted July 1, 2019, date of publication July 8, 2019, date of current version July 26, 2019.

Digital Object Identifier 10.1109/ACCESS.2019.2927427

Anti-Disturbance Neural-Sliding Mode Control for Inertially Stabilized Platform With Actuator Saturation

ZHUSHUN DING[1,2], FENG ZHAO[2], YUEDONG LANG[2], ZHE JIANG[2], AND JIAJING ZHU[2]

[1]Department of Aerospace and Engineering, National University of Defense Technology, Changsha 410073, China
[2]Beijing Institute of Aerospace Control Devices, Beijing 100854, China

Corresponding author: Feng Zhao (zhaofeng_win@126.com)

This work was supported by the National Key Technologies Research and Development Program of China during the 13th Five-Year Plan Period under Grant 2017YFC0601604.

ABSTRACT To consider the environment during ground vehicle driving, the inertially stabilized platform (ISP) can be used for electro-optical tracking instruments to isolate the senor's line of sight (LOS) from the carrier's vibrations with high precision and stability. This paper proposes the combination of a backstepping sliding mode controller with the adaptive neural networks approach (BSMC-NN) for ISP that achieves output torque saturation and considers parametric uncertainties, friction, and gimbal mass imbalance. An adaptive radial basis function neural network is adopted to approximate uncertain disturbances in this dynamic system. In contrast to the existing saturated control structures, an auxiliary function is designed to compensate for any error between the designed and the actual control torque. The closed-loop stability and asymptotic convergence performance are guaranteed based on the Lyapunov stability theory. Finally, the simulation and experimental results demonstrate that this proposed controller can effectively regulate the gimbal rotation angle under different external disturbances. This offers superior control performance despite the existence of the nonlinear dynamics and control input constraints.

INDEX TERMS Backstepping, adaptive RBFNN, mass imbalance, actuator saturation.

I. INTRODUCTION

Due to increasing expectations for unmanned intelligence, surveillance, and reconnaissance systems, the inertially stabilized platform (ISP) attracted significant interest in the aircraft vehicle industry [1], [2]. For example, in the field of civil aerial remote sensing system, the high-precision ISP is indispensable for the stabilization of the axis of optical sensors in space to return the high quality geographic images in real time [3]. In [4], the ISP installed with the optical imaging sensors was mounted beneath the unmanned helicopter to locate faults of a high-voltage line. In the military field, the detector of an optics seeker is positioned on a gyro-stabilized platform which is used for precise missile guidance systems to acknowledge and track targets [5]. Moreover, the automatic gun-turret is mounted on a mobile vehicle to improve the efficiency of extensive artillery firepower and improve the survival ability on the battlefield [6]. Since an important feature of ISPs with optical payloads is the tracking of both fixed or moving targets, the control system should not only have high accuracy but also possess an excellent line-of-sight (LOS) control performance.

Conventional LOS stabilization techniques are implemented with a two-degree of freedom gimbal platform, and the vision sensor and gyros are mounted as close as possible to the gimbal bore-sight on the inner frame axes. The gyro is used to sense the rate disturbances of the LOS in two directions of interest, whose signals are regard as feedback to torque motors and act on the gimbals that attenuate the external disturbance. Furthermore, kinematic coupling needs to be consider in the unmanned aircrafts, as well as the elevation gimbal; and the azimuth gimbal of ISP system [7]. Major outer disturbance sources are the platform base's angular motion, the wind and air-steam induced torque, and the inner disturbances derived from mass imbalance, friction in joints, and gyro signal random drift [8]. To isolate the angular vibration and attenuate the impact of these disturbances, researchers have focused on LOS control algorithms for ISP system [9]–[11]. Various methods have been proposed, ranging from a PID control technique to highly

The associate editor coordinating the review of this manuscript and approving it for publication was Wei Wei.

advance linear and nonlinear control techniques, including LQG control [12], adaptive control [13], H∞ control [14], and hybrid control [15].

In ISP, the inevitable presence of parametric uncertainties and the dynamic mass unbalance may reduce the vibration attenuation performance during the tracking process. However, previous studies have not consider these issues. To overcome this problem, many different control techniques have been reported. Sliding mode control (SMC) [16]–[19] is a well-known nonlinear control strategy for uncertain systems that are affected by unmeasurable disturbances. The linear SMC surface is used to guarantee asymptotic stability and faster convergence time of the system by adjusting the parameters of the sliding surface. However, the high-frequency chattering phenomenon is a severe problem of SMC and is caused by the large gain of the switching function [20]. A robust feedback controller is presented to solve the dynamic mass unbalance of a two-axis gimbal sensor system, and an extended state observer is implemented to obtain an estimate of unmeasured states as well as external disturbances [21]. In [22], active disturbance rejection control (ADRC) was applied to realize control performance with high stabilization precision for ISP. In [23], a composite adaptive fuzzy PID control strategy was developed for a LOS stabilized and tracking turntable under the system uncertainty. However, the construction of a fuzzy rule set depends on the experience of engineers. With a step-by-step recursive process, significant attention has been directed to adaptive backstepping control using a neural network approach over the past decade. Adaptive NN control theory has helped to solve problems in highly nonlinear uncertain systems in a number of research fields [24]–[27]. The radial basis function neural network (RBFNN) offers the advantages of simple structure, fast learning, and better universal approximation capabilities, and an adaptive NN controller can be designed without significant prior knowledge of the system dynamics while avoiding the above mentioned issues. In [28], an adaptive decoupling control was developed based on NNs to improve the tracking and stabilization performance of the three-axis gyro stabilized platform, and NNs were used to compensate for disturbances and uncertainties.

However, in practical cases, an ISP-driven motor likely only provides limited control torque, and actuator saturation is a further problem that requires investigation. Input saturation with a nonlinear factor may degrade system performance and can even lead to system instability [29]–[31]. Several control schemes with actuator saturation have been proposed at the controller design stage. In [32], the command filtered approach was used to ensure both stability and tracking performance of the mirror-stabilized system under input saturation. A bounded virtual control law combined with a linear saturation function was proposed and the global stability of the ISP system can be guaranteed in the presence of input saturation if both controller and anti-windup compensator are simultaneously computed [33]. In [34], an inverse optimal controller with input saturations was designed to achieve asymptotic convergence to the desired attitude and avoid the unwinding phenomenon. Few prior studies considered the motor torque saturation in the ISP system as a nonlinear problem. Consequently, this paper introduces an auxiliary function during nonlinear controller design and analyzes the effect of actuator saturation.

Most of the previous works have assumed that the systems of concern are linear and that the ISP model states are exactly known. Additionally, several parameters, such as the rotational inertia of the platform, are assumed to have a fixed value, which is not the case for physical systems in reality when the camera adjusts the focal length. Motivated by these observations, this paper proposes a backstepping sliding mode controller combined with an adaptive neural networks approach (BSMC-NN) for ISP that has output torque saturation and a number of nonlinear factors; (e.g, friction significantly affects the system behavior). RBFNN approximation is used to overcome system dynamic model uncertainties and unpredictable external disturbances, whose closed loop system will have a quick dynamic response and small overshot. To alleviate the presence of actuator saturation, an auxiliary design function is employed to compensate for any error between the designed and the actual control torque. Both the update laws of the weighting matrix and the asymptotic stability of the closed loop system are derived based on the Lyapunov stability theory. Finally, the effectiveness of the proposed control approach is validated via both simulations and experiments under different disturbed conditions.

The remainder of this paper is organized as follows: Section 2 describes the dynamic model of ISP with mass imbalance and friction disturbance. Section 3 develops the backstepping sliding mode controller based on the compound algorithms of the RBFNN. To validate the proposed method, the detailed simulation procedure of the BSMC-NN controller is presented in section 4, which also describes the experiments. Finally, section 5 concludes this paper.

II. PROBLEM FORMULATION

A. SYSTEM CONFIGURATION

The classical configuration of a two-axis ISP mainly consist of inner and outer gimbal frames, torque motors and gyros. A variety of payloads, including the visible light camera, infrared camera, and laser sensor, that require stabilization are placed on the inner gimbal, where the rate gyro is also placed to measure the rotational rates in two directions of interest. Moreover, two encoders are mounted on two gimbals, respectively, to provide angle displacements of both gimbals. As previously mentioned, the ultimate goal of the control system is to mitigate the disturbances from the mobile carrier motion, while the motors that are directly mounted onto the gimbal axes and sensors respond to vehicle vibration. In other words, the controller ensures the accurate orientation of the visual axis of payloads, which can continuously obtain focused images.

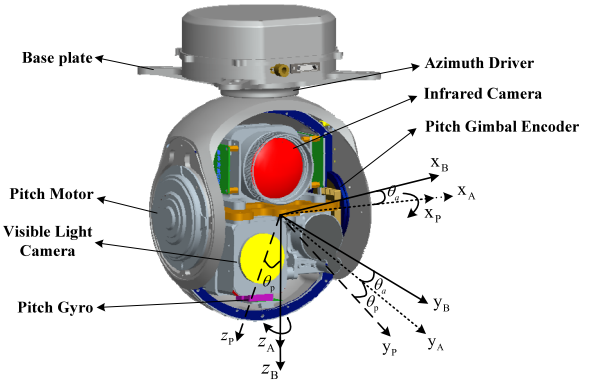

FIGURE 1. Two-gimbal ISP configuration and reference frames.

The right-handed orthogonal coordinate frame is represented by triads of vectors $\{x, y, z\}$. The body-fixed frame (B) is carried into coincidence with the azimuth frame (outer gimbal) (A) by the positive angle θ_a about the z_B axis. The azimuth frame (A) is carried into coincidence with the elevation frame (inner gimbal) (P) by a positive angle of rotation θ_p about the x_P axis. LOS elevation control is exercised by the inner gimbal x_P axis. The attitudes angle of the LOS of the optical payload are defined as $\boldsymbol{\theta}_P^G = [\theta_{Px}^G, \theta_{Py}^G, \theta_{Pz}^G]^T$ with respect to geographic coordinate.

The sequence of both key rotations that express the pose of the elevation gimbal with respect to the base is visualized in Fig.1.

The coordinate transformation from the base frame coordinate (B) to the yaw gimbal coordinate (A) is given by the following rotation matrix.

$$\boldsymbol{R}_B^A = \begin{bmatrix} \cos\theta_a & \sin\theta_a & 0 \\ -\sin\theta_a & \cos\theta_a & 0 \\ 0 & 0 & 1 \end{bmatrix} \tag{1}$$

In a similar way, the coordinate transformation from the yaw gimbal (A) to the elevation gimbal (P) is given by the following rotation matrix.

$$\boldsymbol{R}_A^P = \begin{bmatrix} 1 & 0 & 0 \\ 0 & \cos\theta_p & \sin\theta_p \\ 0 & -\sin\theta_p & \cos\theta_p \end{bmatrix} \tag{2}$$

Now, the following notation is introduced to deduce the angular velocity behavior with the inertial space in frames (B), $(A)$and (P) respectively.

$$\begin{aligned} \boldsymbol{\omega}_B &= \begin{bmatrix} \omega_{Bx} & \omega_{By} & \omega_{Bz} \end{bmatrix}^T \\ \boldsymbol{\omega}_A &= \begin{bmatrix} \omega_{Ax} & \omega_{Ay} & \omega_{Az} \end{bmatrix}^T \\ \boldsymbol{\omega}_P &= \begin{bmatrix} \omega_{Px} & \omega_{Py} & q\omega_{Pz} \end{bmatrix}^T \end{aligned} \tag{3}$$

Using (3), the outer gimbal angular velocity vector $\boldsymbol{\omega}_A$ can be expressed in terms of the base body rate vector $\boldsymbol{\omega}_B$, which gives

$$\boldsymbol{\omega}_A = \boldsymbol{R}_B^A \boldsymbol{\omega}_B + \boldsymbol{\eta} \tag{4}$$

where $\boldsymbol{\eta} = \begin{bmatrix} 0 & 0 & \dot{\theta}_a \end{bmatrix}^T$, and $\dot{\theta}_a = \omega_{Az} - \omega_{Bz}$.

The outer coordinate frame rate vector $\boldsymbol{\omega}_A$ is related to the inner coordinate frame rate vector $\boldsymbol{\omega}_P$, by

$$\boldsymbol{\omega}_P = \boldsymbol{R}_A^P \boldsymbol{\omega}_A + \boldsymbol{\varepsilon} \tag{5}$$

where $\boldsymbol{\varepsilon} = \begin{bmatrix} \dot{\theta}_p & 0 & 0 \end{bmatrix}^T$, and $\dot{\theta}_p = \omega_{Px} - \omega_{Ax}$.

It is assumed that each gimbal is a rigid body and that the gimbal device follow a non-symmetric mass distribution with respect to the rotation axes. The inertia moment matrix of the inner and outer gimbals relative to their respective coordinate frames are

$$\boldsymbol{J}_P = \begin{bmatrix} I_{xx} & I_{xy} & I_{xz} \\ I_{xy} & I_{yy} & I_{yz} \\ I_{xz} & I_{yz} & I_{zz} \end{bmatrix}, \quad \boldsymbol{J}_A = \begin{bmatrix} O_{xx} & O_{xy} & O_{xz} \\ O_{xy} & O_{yy} & O_{yz} \\ O_{xz} & O_{yz} & O_{zz} \end{bmatrix} \tag{6}$$

where I_{xx}, I_{yy}, and I_{zz} represent the elevation gimbal moments of inertia about x, y, and z axes and I_{xy}, I_{xz}, and I_{yz} represent the elevation gimbal moments product of inertia. O_{xx}, O_{yy}, and O_{zz} represent the pitch gimbal moments of inertia about x, y, and z axes and O_{xy}, O_{xz}, and O_{yz} represent the azimuth gimbal moments product of inertia. The platform dynamic model can be obtained via Euler's moment equations for the inner and outer coordinate frames of the gimbal mechanical system. The total torque $\boldsymbol{T}_P$ applied to the inner gimbal is given by Eq.(7):

$$\boldsymbol{T}_P = \frac{d}{dt}\boldsymbol{H}_P + \boldsymbol{\omega}_P \times \boldsymbol{H}_P \tag{7}$$

where the angular momentum $\boldsymbol{H}_P$ is defined as

$$\boldsymbol{H}_P = \boldsymbol{J}_P \boldsymbol{\omega}_P = \begin{bmatrix} I_{xx}\omega_{Px} + I_{xy}\omega_{Py} + I_{xz}\omega_{Pz} \\ I_{xy}\omega_{Px} + I_{yy}\omega_{Py} + I_{yz}\omega_{Pz} \\ I_{xz}\omega_{Px} + I_{yz}\omega_{Py} + I_{zz}\omega_{Pz} \end{bmatrix} \tag{8}$$

By substituting (4) and (5) into (7), the inner gimbal total torque is:

$$\begin{aligned} T_{Px} = {} & I_{xx}\dot{\omega}_{Px} + I_{yz}(\omega_{Py}^2 - \omega_{Pz}^2) + (I_{zz} - I_{yy})\omega_{Py}\omega_{Pz} \\ & + I_{xy}(\dot{\omega}_{Py} - \omega_{Px}\omega_{Pz}) + I_{xz}(\dot{\omega}_{Pz} + \omega_{Px}\omega_{Py}) \end{aligned} \tag{9}$$

Then the Eq.(9) can be rewritten as:

$$I_{xx}\dot{\omega}_{Px} = T_{Px} + T_{Pe} + T_{Pc} + T_{Pd} \tag{10}$$

where T_{Px} represents the control torque driven by the elevation frame actuator and consider the Eq.(9) and Eq.(10), the terms T_{Pe}, T_{Pc} and T_{Pd} can be obtained by

$$\begin{aligned} T_{Pe} = {} & -(I_{xy}\sin\theta_p + I_{xz}\cos\theta_p)(\dot{\omega}_{Az} + \omega_{Ax}\omega_{Ay} - \omega_{Ay}) \\ & + (I_{xy}\cos\theta_p - I_{xz}\sin\theta_p)\omega_{Ax}\omega_{Az} \\ & + \left[(I_{yy} - I_{zz})\cos 2\theta_p - 2I_{yz}\sin 2\theta_p\right]\omega_{Ay}\omega_{Az} \\ & + \frac{1}{2}\left[2I_{yz}\cos\theta_p + (I_{yy} - I_{zz})\sin 2\theta_p\right]\omega_{Az}^2 \end{aligned} \tag{11}$$

$$\begin{aligned} T_{Pc} = {} & (I_{xz}\sin\theta_p - I_{xy}\cos\theta_p)(\dot{\omega}_{Ay} + \omega_{Az}) \\ & + \frac{1}{2}\left[(I_{yy} - I_{zz})\sin 2\theta_p - 2I_{yz}\cos\theta_p\right]\omega_{Ay}^2 \end{aligned} \tag{12}$$

$$\begin{aligned} T_{Pd} = {} & (I_{xy}\omega_{Az}\cos\theta_p - I_{xy}\omega_{Ay}\sin\theta_p - I_{xz}\omega_{Ay}\cos\theta_p \\ & - I_{xz}\omega_{Az}\sin\theta_p)\dot{\theta}_p \end{aligned} \tag{13}$$

where the terms T_{Pe} and T_{Pc} represent the cross-coupling term caused by outer frame rotations, and T_{Pd} is regarded as the disturbance of the inner elevation gimbal motion relative to the azimuth frame.

Since the inner frame is the elevation gimbal, the inertial angular momentum of the outer gimbal is the sum of elevation and azimuth frames, and can be given by:

$$\boldsymbol{H}_A = \boldsymbol{J}_A \boldsymbol{\omega}_A + \boldsymbol{R}_P^A H_P \tag{14}$$

In a similar manner, the rigid frame driven torque for the azimuth gimbal is derived from

$$I_A \dot{\omega}_{Az} = T_{Az} \cos\theta_P + T_{Ae} + T_{Ac} + T_{Ad} \tag{15}$$

With

$$I_A = O_{zz} + I_{zz} \sin^2\theta_p + I_{yy} \cos^2\theta_p - I_{zy} \sin 2\theta_p \tag{16}$$

$$\begin{aligned} T_{Ae} = {} & \Big[O_{xx} - O_{yy} - I_{xx} + I_{zz} \cos^2\theta_p + I_{yy} \sin^2\theta_p \\ & + I_{yz} \sin 2\theta_p\Big] \omega_{Ax} \omega_{Az} \cos\theta_p \end{aligned} \tag{17}$$

$$\begin{aligned} T_{Ac} = {} & -\left[O_{xz} + \frac{1}{2}(I_{yy} - I_{zz}) \sin 2\theta_p + I_{yz} \cos 2\theta_p\right] \\ & \times (\dot{\omega}_{Az} - \omega_{Ax}\omega_{Ay}) \cos\theta_p \\ & - (O_{yz} + I_{xy} \cos\theta_p - I_{xz} \sin\theta_p)(\dot{\omega}_{Ax} + \omega_{Az}\omega_{Ay}) \cos\theta_p \\ & - (O_{xy} + I_{xz} \cos\theta_p - I_{xy} \sin\theta_p)(\omega_{Az}^2 - \omega_{Ax}^2) \cos\theta_p \\ & + \dot{\omega}_{Az} \sin\theta_p - \omega_{Px}\omega_{Ax} \end{aligned} \tag{18}$$

$$\begin{aligned} T_{Ad} = {} & \theta_a \dot{\theta}_p \cos\theta_p [(I_{zz} - I_{yy})(\omega_{Az} \cos 2\theta_p - \omega_{Ay} \sin 2\theta_p) \\ & + 2I_{yz}(\omega_{Az} \sin 2\theta_p + \omega_{Ay} \cos 2\theta_p) \\ & + (I_{xy} \sin\theta_p + I_{xz} \cos 2\theta_p)(\omega_{Ax} + \omega_{Py}) - I_{xx}\omega_{Az}\theta_a] \\ & + \omega_{Px}\omega_{Py} \end{aligned} \tag{19}$$

where T_{Az} represents the control torque driven by the azimuth frame actuator. T_{Ae} and T_{Ac} can be interpreted as the influence of the dynamic unbalance inertia matrix. T_{Ad} represents the cross-coupling term generated by the inner elevation gimbal motion relative to the azimuth frame.

B. ACTUATOR MODEL

Brush less DC torque motors are used for both inner and outer gimbals. Using Newton's law, the dynamic model of the direct drive motors can be described by

$$J_l \frac{d\omega_l}{dt} = T_l - T_{d_l} \tag{20}$$

$$T_l = K_T i_a \tag{21}$$

where ω_l represents the angular speed, for the inner gimbal $\omega_1 = \omega_{Px}$ and for the outer gimbal $\omega_2 = \omega_{Az}$; i_a represents the current flowing through the motor; T_{d_l} represents the external disturbance torque and defined as $T_{d_l} = T_{im} + T_F$ in which T_{im} represents the mass imbalance disturbance and T_F is the friction disturbance; The inertia of gimbal J_l was obtained by Solid Works.

The electrical circuit equation is

$$L_a \frac{di_{ai}}{dt} + R_a i_{ai} + K_b \omega_{li} = u_{ai} \quad i = 1, 2 \tag{22}$$

where K_b represents the back EMF constant, and the voltage u_{ai} represents produced by the drive controller. In many instances, the rotor inductance L_a can be neglected. The parameter torque constant K_T and the resistance of the motor R_a are provided by the motor manufacturer.

C. MODELING FOR MASS IMBALANCE DISTURBANCE

In reality, the center of gravity (CG) of the platform is not on the pivot point of the rotating gimbal, and there is an offset r_1 due to the lever arm between gimbal pivot point and the plat form CG. This lever arm can cause mass imbalance torque about the pivot point. Dynamic mass imbalance torque occurs when the ISP is working in stability mode, where the pitch gimbal is maintained in the level direction of the local geographic coordinate. Then, the lever arm almost remains level all the time.

The dynamic mass imbalance disturbance torque T_{im} can be expressed as

$$T_{im} = mr_1(g + a_z) - mr_0 r_1 \dot{\theta}_b^2 \cos(\theta_b + \delta) \tag{23}$$

where r_0 represents the distance between the pivot point and the base CG; θ_b represents the base angle related to the reference axis; a_z represents the vertical acceleration of the base; m represents the total mass of both gimbal and payload.

D. FRICTION MODEL

To accurately capture the dynamic response of the ISP, the Stribeck model is adopted to describe the static and dynamic friction in the inertial stabilized platform system. When the gimbal is rotating at very low angular velocity, the Stribeck model reflects the decreasing friction with increasing motion speed. The Stribeck model is given as [10]:

$$T_F = \left[M_c + (M_s - M_c)\, e^{-\left(\frac{\omega}{\omega_s}\right)^2}\right] \mathrm{sgn}(\omega) + \sigma\omega \tag{24}$$

where M_c represents the coulomb friction torque; M_s represents the maximum static friction; ω represents the relative angular velocity between contact surfaces; σ represents viscous friction coefficient; ω_s represents the Stribeck velocity.

E. PROBLEM STATEMENT

ISP can be used to switch several times between two working modes, attitude servo-control (used to realize target searching and tracking) and attitude locking (used to attenuate external disturbances that are transmitted to the optical payload); therefore, this study focuses on the angle velocity ω_{Px} and ω_{Az}. The rotation attitude angle of the gimbal with respect to the geographic coordinate θ_{Px}^G and θ_{Pz}^G can reflect the vibration situation of the camera. The stabilization of the pitch and azimuth axis can be realized in the same pattern since they have similar representations. Additionally, the stabilization loop band width must be sufficiently high to reject the platform disturbance spectrum. To develop the anti-disturbance SMC control method using the NN technique for ISP, the dynamic equations for the ISP system

from (10) and (15) are expressed as follows:

$$\begin{aligned}\dot{x}_1 &= x_2\\ \dot{x}_2 &= f_1(t) + b_1 T_{Px} + d_1(t)\\ \dot{x}_3 &= x_4\\ \dot{x}_4 &= f_2(t) + b_2 T_{Az} + d_2(t)\end{aligned} \tag{25}$$

where $x_1 = \theta^{\mathrm{G}}_{\mathrm{Px}}, x_2 = \omega_{Px}, x_3 = \theta^{\mathrm{G}}_{\mathrm{Pz}}, x_4 = \omega_{Az}$. In addition, combined with Eqs. (11),(13) and (17), the system function is defined as

$$f_1(t) = \frac{T_{Pe} + T_{Pc}}{I_{xx}}, \quad b_1 = \frac{1}{I_{xx}}, \quad d_1(t) = \frac{T_{Pd}}{I_{xx}}$$
$$f_2(t) = \frac{T_{Ae} + T_{Ac}}{I_A}, \quad b_2 = \frac{\cos\theta_P}{I_A}, \quad d_2(t) = \frac{T_{Ad}}{I_A}$$

To solve these parameter uncertainties and obtain a more applicable solution, the parameters in Eq. (24) are not exactly known which could be represented by

$$F_1 = \Delta f_1(t) + \Delta b_1 T_{Px} + d_1(t) \tag{26}$$
$$F_2 = \Delta f_2(t) + \Delta b_2 T_{Az} + d_2(t) \tag{27}$$

where Δ denotes system uncertainties. As discussed in the above analysis, the motor torque of the ISP system is subject to amplitude saturation, which should be explicitly considered for the controller design. For ISP with dynamic model parameter uncertainties and mass imbalance, an adaptive control input T_{u} is required to stabilize the LOS of closed loop systems due to the influence of external disturbances, to maintain high performance during actuator saturation.

Considering the presence of the motor torque saturation constraint on T_{u}, $|T_{\mathrm{u}}| \le T_{\max}$ can be set, where $T_{\max}$ is the constraint of the known upper limit of the force. Thus, the control input force T_{u} is defined by:

$$T_{\mathrm{u}} = \begin{cases} T_{\max} & if\ T_c \ge T_{\max} \\ T_c & if\ -T_{\max} \le T_c \le T_{\max} \\ -T_{\max} & if\ T_c \le -T_{\max} \end{cases} \tag{28}$$

where T_c represents the designed control law.

To design effective control schemes, the following lemmas and assumptions are applied throughout the paper.

Lemma [28]: Let $g(x)$ be a continuous function, which is defined over a compact set D. Then, there exists a neural network system $W^{\mathrm{T}}\Theta(x)$ which can approximate $g(x)$ with arbitrary accuracy, so that

$$g(x) = W^{\mathrm{T}}\Theta(x) + \varepsilon \tag{29}$$

where $W = [w_1, w_2, \cdots, w_N]^{\mathrm{T}}$ represents the ideal constant weight vector, $\Theta(x) = [\Theta_1(x), \Theta_2(x), \cdots, \Theta_N(x)]^{\mathrm{T}}$ is the RBFs vector, $N > 1$ represents the number of the neurons, and ε is the approximation error which is minimized by the ideal vector W:

$$W := \underset{W\in\mathbb{R}}{\operatorname{argmin}} \left\{ \sup_{x\in D} \left| g(x) - W^{\mathrm{T}}\Theta(x) \right| \right\}$$

Assuming that ε is smaller than a small positive constant ε^*, then $|\varepsilon| < \varepsilon^* < \infty$ with ε^* being an unknown positive constant. $\Theta_i(x)$ is a Gaussian function,

$$\Theta_i(x) = \exp\left[\frac{-(x-\mu_i)^{\mathrm{T}}(x-\mu_i)}{\eta_i^2} \right] \tag{30}$$

where $\mu_i = [\mu_{i1}, \mu_{i2}, \cdots, \mu_{in}]^{\mathrm{T}}$ and η_i represent the centers and widths of the Gaussian functions, respectively. n is the dimension of x.

Assumption 1: The ISP disturbance uncertainty F is bounded. i.e. $|F| \le \overline{F}$.

Assumption 2: The desired $x_{\theta\_\mathrm{desire}}$ of the ISP is a reference trajectory which is available to design a feasible control scheme in the presence of parametric uncertainties, external disturbance and torque saturation. $\dot{x}_{\theta\_\mathrm{desire}}$ and $\ddot{x}_{\theta\_\mathrm{desire}}$ exist. For any arbitrary $t > 0$, there exists $\delta_{11} > 0$ and $\delta_{21} > 0$ so that $\left\|\dot{x}_{\theta\_\mathrm{desire}}\right\| < \delta_{11}$ and $\left\|\ddot{x}_{\theta\_\mathrm{desire}}\right\| < \delta_{21}$.

III. ANTI-DISTURBANCE NEURAL NETWORK SMC CONTROLLER DESIGN

For the desired angle tracking objective, a generalized tracking state is defined as $z_1 = x_1 - x_{\theta\_\mathrm{desired}}$, hence, the derivative of z_1 is: $\dot{z}_1 = \dot{x}_1 - \dot{x}_{\theta\_\mathrm{desired}}$.

Step 1: A virtual control law α_1 is introduced and the second error variable is defined as $z_2 = x_2 - \alpha_1$, where $\alpha_1 \in \mathbb{R}$. The parameter α_1 is defined as:

$$\alpha_1 = -K_1 z_1 + \dot{x}_{\theta\_\mathrm{desired}} \tag{31}$$

where the gain coefficient $K_1 \in \mathbb{R}^+$, and the time derivative of z_1 is obtained by:

$$\dot{z}_1 = z_2 + \alpha_1 - \dot{x}_{\theta\_\mathrm{desired}} = z_2 - K_1 z_1 \tag{32}$$

Considering a first Lyapunov function candidate $V_1 = \frac{1}{2}z_1^2$, the time derivative of V_1 is:

$$\dot{V}_1 = -K_1 z_1^2 + z_1 z_2 \tag{33}$$

Step 2: Differentiating $z_2 = x_2 - \alpha_1$ with respect to time, provides $\dot{z}_2 = \dot{x}_2 - \dot{\alpha}_1$. Eq. (25) is substituted into this to obtain:

$$\dot{z}_2 = f(t) + b_1 T_{\mathrm{u}} + F_1 - \dot{\alpha}_1 \tag{34}$$

To let the state error of angular velocity loop z_2 converge to zero, sliding mode control is applied to system parameter variations and external disturbances. The sliding mode surface is introduced to design control T_{u} to improve the ISP tracking response and precision, which are designed with a positive constant c_1 as follow:

$$s = c_1 z_1 + z_2 \tag{35}$$

A switching control term can be used in the SMC controller to drive the system states toward the sliding surface from any initial state condition. As the state approach the sliding surface, the equivalent control is applied to maintain the trajectory of the system state in the absence of uncertainties and external disturbances.

From Eq. (35), the $\dot{s}$ is given by

$$\dot{s} = c_1\dot{z}_1 + \dot{z}_2 = c_1\dot{z}_1 + f(t) + b_1T_u + F_1 - \dot{\alpha}_1 \quad (36)$$

The following auxiliary design system [49] is used to analyze the effects of actuator saturation.

$$\dot{\zeta} = \begin{cases} -K_\lambda\zeta - \dfrac{|b_1 s\Delta\tau| + 0.5\Delta\tau^2}{\zeta} + \Delta\tau & |\zeta| \geq \mu \\ 0 & |\zeta| < \mu \end{cases} \quad (37)$$

where $\Delta\tau = T_u - T_c$, $K_\lambda \in \mathbb{R}^+$, μ is a small positive value and $\zeta \in \mathbb{R}$ is the auxiliary design system state.

A second Lyapunov function candidate is considered:

$$V_2 = V_1 + \frac{1}{2}s^2 + \frac{1}{2}\zeta^2 \quad (38)$$

Invoking Eq. (13) and (14), the time derivative of V_2 is:

$$\begin{aligned}\dot{V}_2 &= -K_1z_1^2 + z_1z_2 + s\dot{s} + \zeta\dot{\zeta} \\ &= -K_1z_1^2 + z_1z_2 + s\left[c_1\dot{z}_1 + f(t) + b_1T_u + F_1 - \dot{\alpha}_1\right] \\ &\quad -K_\lambda\zeta^2 - |b_1s\Delta\tau| - 0.5\Delta\tau^2 + \zeta\Delta\tau \end{aligned} \quad (39)$$

Due to $\zeta\Delta\tau \leq \frac{1}{2}\zeta^2 + \frac{1}{2}\Delta\tau^2$, we obtain:

$$\begin{aligned}\dot{V}_2 \leq -K_1z_1^2 + z_1z_2 + s\left[c_1\dot{z}_1 + f(t) + b_1T_u + F_1 - \dot{\alpha}_1\right] \\ -K_\lambda\zeta^2 - |b_1s\Delta\tau| + 0.5\zeta^2 \end{aligned} \quad (40)$$

Since $T_u = T_c + \Delta\tau$, it can be substituted for the inequality in Eq. (18) to obtain,

$$\begin{aligned}\dot{V}_2 &= -K_1z_1^2 + z_1z_2 + s\left[c_1\dot{z}_1 + f(t) + b_1T_c + F_1 - \dot{\alpha}_1\right] \\ &\quad -(K_\lambda - 0.5)\zeta^2 + b_1s\Delta\tau - |sb_1\Delta\tau| \\ &\leq -K_1z_1^2 + z_1z_2 + s\left[c_1\dot{z}_1 + f(t) + b_1T_c + F_1 - \dot{\alpha}_1\right] \\ &\quad -(K_\lambda - 0.5)\zeta^2 \end{aligned} \quad (41)$$

By considering the actuator saturation effect, the control law can be designed as:

$$\begin{aligned}T_c &= -\frac{1}{b_1}\left[f(t) + c_1\dot{z}_1 + z_1 + \overline{F}_1\mathrm{sgn}(s) - \dot{\alpha}_1\right. \\ &\quad \left. + h\left(s - \zeta + \varphi\mathrm{sgn}(s)\right)\right] \\ &= -\frac{1}{b_1}\left[f(t) + c_1\dot{z}_1 + z_1 + h(s-\zeta) - \dot{\alpha}_1\right. \\ &\quad \left. + (\overline{F}_1 + h\varphi)\mathrm{sgn}(s)\right] \end{aligned} \quad (42)$$

where h and φ are positive constants. Substituting (42) into (40), obtains the following equation:

$$\begin{aligned}\dot{V}_2 = -(K_1 + c_1)z_1^2 - hs^2 - h\varphi|s| + F_1s \\ -\overline{F}_1|s| - (K_\lambda - 0.5)\zeta^2 + h\zeta s \end{aligned} \quad (43)$$

Due to $h\zeta s \leq \frac{1}{2}s^2 + \frac{1}{2}h^2\zeta^2$,

$$\begin{aligned}\dot{V}_2 \leq -(K_1 + c_1)z_1^2 - (h - 0.5)s^2 - h\varphi|s| \\ -(K_\lambda - 0.5h^2 - 0.5)\zeta^2 \end{aligned} \quad (44)$$

Choosing appropriate parameters $K_1, \varphi, c_1, h, K_\lambda$, can guarantee that $\dot{V}_2 \leq 0$. Due to the switching action terms $(\overline{F}_1 + h\varphi)\mathrm{sgn}(s)$, there inevitably exist chatting phenomenon. Moreover, ISP is complicated by nonlinearities and uncertainties in the system dynamic, therefore, in this case, the exact $\Delta f_1(x,t)$, $\Delta b_1, d_1(t)$ may remain unknown. An adaptive RBFNN is used to approximate these uncertainties in the dynamic model. This is valid in practical digital processing since the sampling estimation period is sufficiently short compared to the variations of W and ε.

According to Lemma, it can be suggested that:

$$F_1 = W_c^{\mathrm{T}}\Theta(z) + \varepsilon_c \quad (45)$$

where W_c represents the ideal constant weight vector; ε_c represents the approximation error. The control law can be proposed as:

$$\begin{aligned}T_c = -\frac{1}{b_1}\Big[f(t) + c_1\dot{z}_1 + z_1 + h(s-\zeta) - \dot{\alpha}_1 \\ + \hat{W}_c^{\mathrm{T}}\Theta(z) + \hat{\varepsilon}_c\Big] \end{aligned} \quad (46)$$

where $\hat{W}_c$ and $\hat{\varepsilon}_c$ are estimations of the unknown vector W_c and the unknown bounded value ε_c. Therefore:

$$\tilde{W}_c = \hat{W}_c - W_c, \tilde{\varepsilon}_c = \hat{\varepsilon}_c - \varepsilon_c \quad (47)$$

The RBFNN updating law is then defined as:

$$\dot{\hat{W}}_c = = gamma_1s\Theta(z) \quad (48)$$

$$\dot{\hat{\varepsilon}}_c = \gamma_2 s \quad (49)$$

where $\gamma_1 > 0$, and $\gamma_2 > 0$ are chosen by design, and are constant related to the adaption learning rate.

Considering the effect of the error $\tilde{W}_c$ and $\tilde{\varepsilon}_c$ on system stability, the Lyapunov function candidate can be written as $V_2^* = V_2 + \frac{1}{\gamma_1}\tilde{W}_c^{\mathrm{T}}\tilde{W}_c + \frac{1}{\gamma_2}\tilde{\varepsilon}_c^2$, and the derivative of V_2^* is:

$$\begin{aligned}\dot{V}_2^* &= \dot{V}_2 + \frac{1}{\gamma_1}\tilde{W}_c^{\mathrm{T}}\dot{\tilde{W}}_c + \frac{1}{\gamma_2}\tilde{\varepsilon}_c\dot{\tilde{\varepsilon}}_c \\ &= -(K_1 + c_1)z_1^2 - hs^2 - (K_\lambda - 0.5)\zeta^2 \\ &\quad + \left[F_1 - \hat{W}_c^{\mathrm{T}}\Theta(z) - \hat{\varepsilon}_c\right]s \\ &\quad + h\zeta s + \frac{1}{\gamma_1}\tilde{W}_c^{\mathrm{T}}\dot{\hat{W}}_c + \frac{1}{\gamma_2}\tilde{\varepsilon}_c\dot{\hat{\varepsilon}}_c \\ &\leq -(K_1 + c_1)z_1^2 - (h - 0.5)s^2 - (K_\lambda - 0.5h^2 - 0.5)\zeta^2 \\ &\quad + \left[F_1 - \hat{W}_c^{\mathrm{T}}\Theta(z) - \hat{\varepsilon}_c\right]s + \frac{1}{\gamma_1}\tilde{W}_c^{\mathrm{T}}\dot{\hat{W}}_c + \frac{1}{\gamma_2}\tilde{\varepsilon}_c\dot{\hat{\varepsilon}}_c \\ &\leq -(K_1 + c_1)z_1^2 - (h - 0.5)s^2 - (K_\lambda - 0.5h^2 - 0.5)\zeta^2 \\ &\quad -\tilde{W}_c^{\mathrm{T}}\Theta(z)s - \hat{\varepsilon}_cs + \frac{1}{\gamma_1}\tilde{W}_c^{\mathrm{T}}\dot{\hat{W}}_c + \frac{1}{\gamma_2}\tilde{\varepsilon}_c\dot{\hat{\varepsilon}}_c \end{aligned} \quad (50)$$

Substituting the updating law stated in Eq. (48) and (49) into Eq. (50) obtains:

$$\dot{V}_2^* = -(K_1 + c_1)z_1^2 - (h - 0.5)s^2 - (K_\lambda - 0.5h^2 - 0.5)\zeta^2 \quad (51)$$

In order to guarantee closed loop stability, the control parameters $K_1, \varphi, c_1, h, K_\lambda$ should satisfy the following criteria: $K_1 > 0, \varphi \geq 0, c_1 \geq 0, h \geq 0.5$ and $K_\lambda \geq 0.5h^2 + 0.5$. These conditions will ensure that $\dot{V}_2^* \leq 0$. Moreover, by using Barbalat's Lemma [35], it can be shown that s will converge

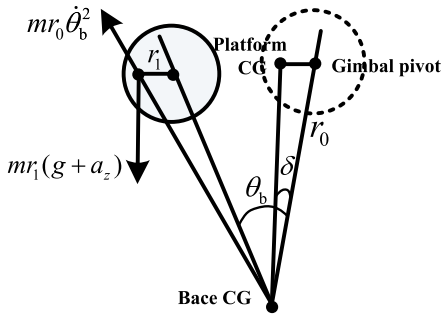

FIGURE 2. Mass imbalance model.

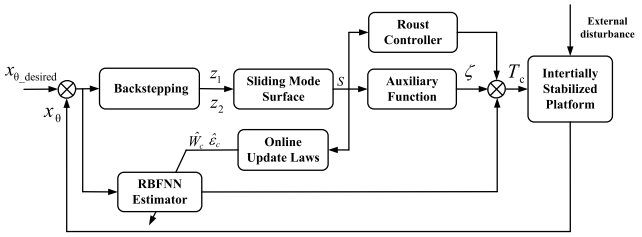

FIGURE 3. Control structure diagram of the ISP system.

to zero as t$\rightarrow\infty$. From the above analysis, it can be shown that $z_1, z_2, \tilde{W}_c$ and $\tilde{\varepsilon}_c$ will asymptotically converge to zero. Consequently, the stability of the proposed adaptive backstepping NNSMC control system can be guaranteed and the attitude angle of the reference trajectory feed forward results in superior tacking performance.

The structural diagram for the proposed controller for ISP is depicted in Fig. 3. The adaptive neural network control development can be summarized by the following theorem.

Theorem: Considering the ISP dynamic description by Eq. (25), under assumption 1-2, with a constraint effect from auxiliary analysis Eq. (37) and a control law Eq. (46) based on adaptive laws Eq. (48)and (49), and given that the full states information is available. For bounded initial conditions, the control parameters $K_1, \varphi, c_1, h, K_\lambda$ should satisfy the following criteria: $K_1 > 0, \varphi \geq 0, c_1 \geq 0, h \geq 0.5$ and $K_\lambda \geq 0.5h^2+0.5$. Then, the closed loop system signals $z_1, z_2, \tilde{W}_c$, and $\tilde{\varepsilon}_c$ will converge to zero as t$\rightarrow\infty$. The closed-loop system error signal $e(t)$ will asymptotically converge to zero.

Proof: See Eqs. (31) $\sim$ (51).

IV. SIMULATIONS AND EXPERIMENT

To validate the efficacy of the proposed control strategy, MATLAB was used to build the attitude servo-control simulation model of the two-axis ISP system which is working under ground vehicle driving, and a number of numerical simulations are performed with actuator saturation. The corresponding mass imbalance torque, friction torque and external disturbances have been considered in the simulation of a real working condition.

The ISP system is mounted with a visible camera, infrared camera and laser scanner, and the total weight of payloads is 3.5 kg. By installing the counterweight, the moment of the center of gravity is less than 3mm, and the base vertical

TABLE 1. Parameter values of the ISP system.

Parameter	Description	Value	Parameter	Description	Value
I_{xx}	The pitch gimbal moments of inertia about x	4×10^{-3} Kg.m^2	K_T	Torque constant	0.3N.m/A
I_{yy}	Pitch gimbal moments of inertia about y	4.8×10^{-3} Kg.m^2	K_b	Back EMF constant	0.3N.m/A
I_{zz}	Pitch gimbal moments of inertia about z	4.9×10^{-2} Kg.m^2	u_{ai}	Peck voltage	28V
O_{xx}	Azimuth gimbal moments of inertia about x	6.4×10^{-3} Kg.m^2	M_c	Coulomb friction torque	0.03N.m
O_{yy}	Azimuth gimbal moments of inertia about y	8.3×10^{-3} Kg.m^2	M_s	Maximum static friction	0.06N.m
O_{zz}	Azimuth gimbal moments of inertia about z	9.8×10^{-3} Kg.m^2	σ	Viscous friction coefficient	0.057N.m/rad/s
R_a	Resistance of the motor	10Ω	ω_s	Stribeck velocity	0.05rad/s

acceleration a_z used in the simulation is obtained from [36] as under the ground vehicle situation. The parameters of the relevant friction can be found in [10]. The elevation and pitch gimbal moments of inertia about x, y, and z axes are listed in Table 1.The maximum value of the actuator output force is restricted to 0.5 Nm.

A. REFERENCE TRAJECTORY AND DYNAMIC STABILITY SIMULATION

System initial conditions are set to $x_1 = 0, \zeta = 0.01$ and the number of neurons in the hidden layer is 50. The initial weighting vectors are selected as $\hat{W}_c^{\mathrm{T}}(0) = \left[0.1\ 0.1\ \cdots\ 0.1\right]^{\mathrm{T}}$ and the centers of the Gaussian function are evenly distributed from $[-1,1]$ and $\eta_n = 8(n = 1, 2, 3 \ldots 50)$.

To evaluate the performance of the designed controller, two typical external disturbances are considered cases in the simulation.

Case 1: Since the resonance frequency of the car body is about 1Hz [37], an external excitation close to this frequency might cause large disturbance amplitudes, which induce LOS oscillation. To test the control performance near this resonance frequency, it is considered as the base of the platform disturbance as

$$\omega_{\mathrm{By}}^{\mathrm{G}}(t) = 1.5\sin 2\pi t \tag{52}$$

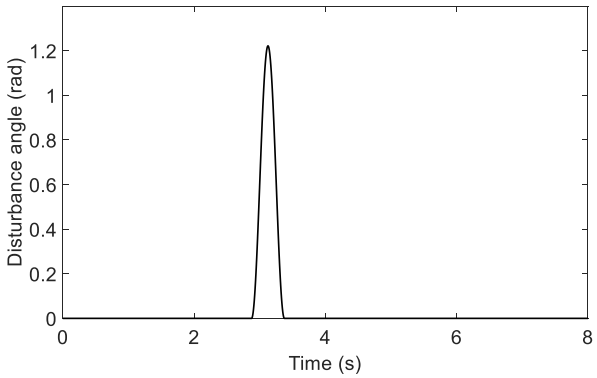

FIGURE 4. Bump disturbance angle.

Case 2: Consider a sinusoidal bump when the vehicle is crossing speed control humps on a road. A mathematical description of this type of the sinusoidal bump is given by

$$o_{\mathrm{By}}^{\mathrm{G}}(t) = \begin{cases} h\left[1 + \sin\left(\dfrac{2\pi}{\mathrm{T_b}}t\right)\right] & \text{if } t_l \le t \le t_h \\ 0 & \text{otherwise} \end{cases} \tag{53}$$

where h represents the height of the bump, and $\mathrm{T_b}$ represents one of the sinusoidal bump periods. Suppose, $h = 1.22$rad, $\mathrm{T_b} = 0.5$s. The corresponding disturbance angle of the platform base is shown in Fig. 4.

In this paper, the visual servo tracking of the ISP system requires target miss distance information based on image processing. The initial attitude angle corresponding to the off-target amount is set to 6°. Consequently, it can keep up the goal of the pre-determined attitude angle trajectory, and helps to adjust the gimbal acceleration to a low level which can achieve high performance. The reference attitude angle trajectory is determined via polynomial expression in Eq.(54).

$$\theta_{\mathrm{desired}}(t) = \begin{cases} a_0 + a_1 t + a_2 t^2 + a_3 t^3 + a_4 t^4, & t \le T_r \\ 0 & t \le T_r \end{cases} \tag{54}$$

where $T_r = 1$s, $a_i, i = 0, 1, 2, 3, 4$ is determined so that

$$\begin{aligned} \theta_{\mathrm{desired}}(0) &= a_0 = \theta_1(0), \quad \dot{\theta}_{\mathrm{b\_desired}}(0) = a_1 = \theta_2(0) \\ \theta_{\mathrm{desired}}(T_r) &= a_0 + a_1 T_r + a_2 T_r^2 + a_3 T_r^3 + a_4 T_r^4 = 0 \\ \dot{\theta}_{\mathrm{desired}}(T_r) &= a_1 + 2a_2 T_r + 3a_3 T_r^2 + 4a_4 T_r^3 = 0 \\ \ddot{\theta}_{\mathrm{desired}}(T_r) &= 2a_2 + 6a_3 T_r + 12a_4 T_r^2 = 0 \end{aligned}$$

In simulations, the backstepping SMC (BSMC) command in Eq. (42) and the traditional SMC controller are also adopted for comparison purposes to validate the performance of the designed controller.

B. COMPARISON OF THE CONTROLLER PERFORMANCE

The pitch gimbal is used as an example to validate the proposed controller, and the dynamic response of the pitch gimbal with sine excitation is shown in Fig. 5(a). The pitch angle position better tracked the target miss distance despite of external disturbances. In the process of tracking the miss distance, the peak tracking angle error is 8 mrad via BSMC control but only 0.9 mrad via adaptive BSMC-NN control.

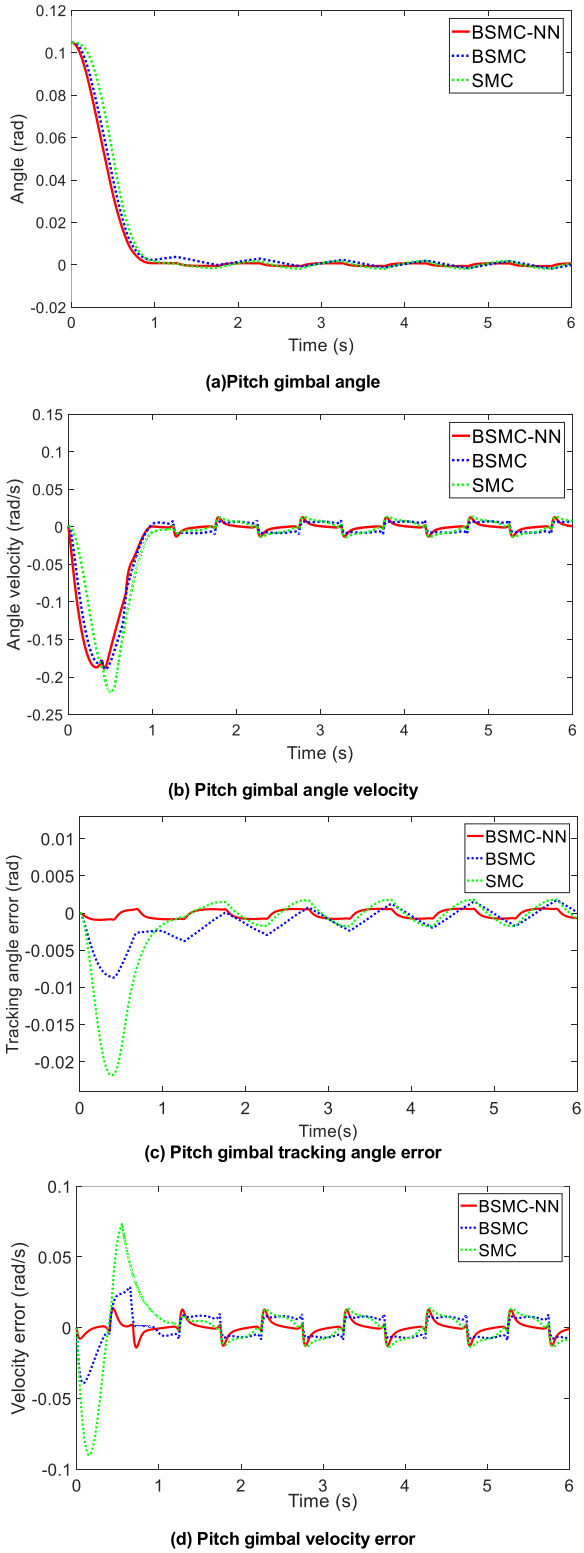

FIGURE 5. Case 1: Pitch gimbal angle, angle velocity, tracking angle error and velocity error.

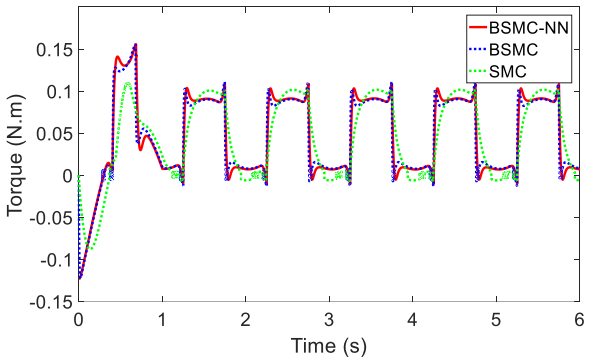

FIGURE 6. Case 1: Motor torque.

In the Fig. 5(b), the minimum angular velocity tracking error is 15 mrad/s via BSMC-NN controller. After 1sec, the RMS value of the pitch angle is 19.2mrad via BSMC, whereas in the case of adaptive BSMC-NN control, it is 17.9 mrad. The RMS values of the angle velocity using the proposed controller, BSMC and SMC control are 39.3, 40.8 and 48.7 mrad/s, respectively. The chattering phenomena of the output torque are apparent in the Fig. 5(a) with BSMC and conventional SMC due to small boundary selected. Clearly, the LOS stability could be significantly improved via adaptive BSMC-NN control.

Bump excitation is used to test the fast tracking responses of the pitch gimbal, and the dynamic response of the gimbal angle position and angle velocity using adaptive BSMC-NN, BSMC and SMC control are shown in Fig. 6. The amplitude of the angle position and angle velocity via adaptive BSMC-NN is smaller and diminishes much faster compared to both BSMC and SMC controllers. The minimum amplitude of the angle position is 3.1 mrad via adaptive BSMC-NN control, which is lower than 1.1 m rad via BSMC control. In addition, the peak-to-peak value of the pitch angle decreased from 7.4 m rad to 5.3 m rad compared to BSMC control. Adaptive BSMC-NN control can suppress 3.2% RMS value of angle velocity, which indicates a 1.9% improvement over SMC control. Thus, adaptive BSMC-NN control with ISP system improves performance more clearly than either BSMC or SMC control.

Fig. 7 shows that the generated motor torques via adaptive BSMC-NN, BSMC and SMC control are saturated within the limits of the actuator under bump external excitations. Although the output torque remains within the constrained range, as presented in Fig. 5 and Fig.6, the adaptive BSMC-NN controller has a superior ability to deal with the nonlinear friction and time-varying ISP system with actuator saturation. The SMC controller may achieve a similar performance, which requires more control torque beyond the output capability of the actuator.

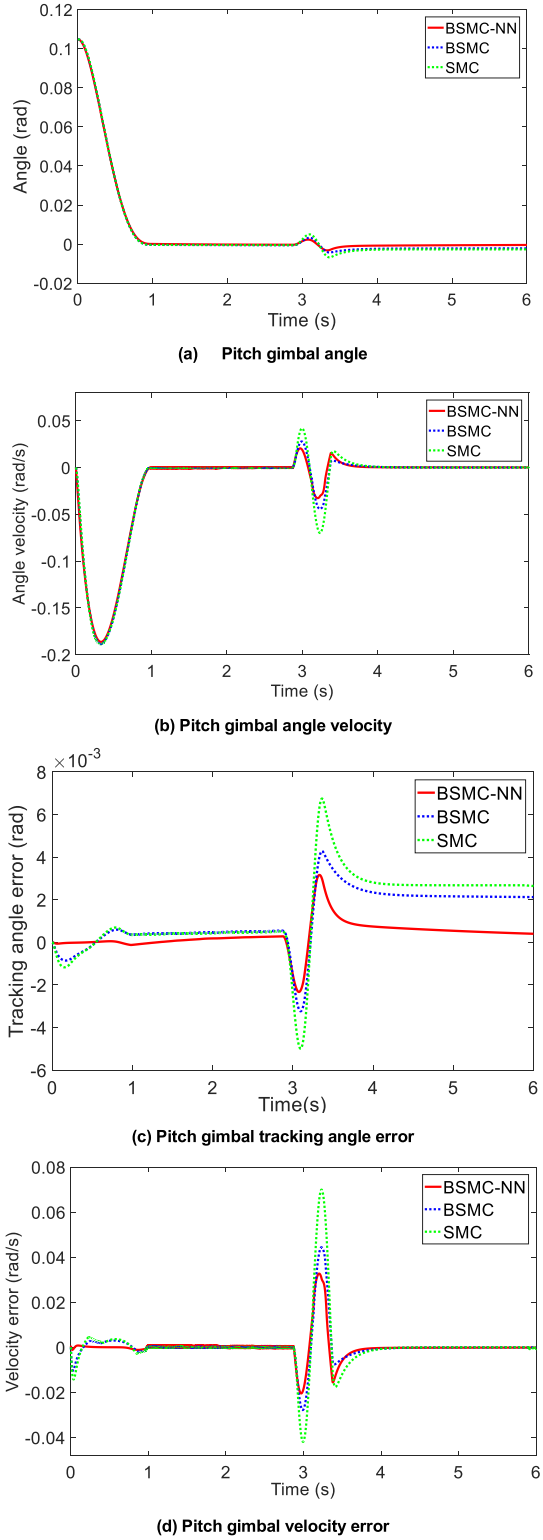

FIGURE 7. Case 2: Pitch gimbal angle, Angle velocity, Tracking angle error and Velocity error.

C. SWING TABLE EXPERIMENTS

The experimental setup for the ISP control system include a two-axis swing platform, power box, data acquisition cards, and personal computer. A larger angular range of the carrier motion can be obtained by the swing plat for m and the sinusoidal disturbance environment is used to validate the proposed control algorithm. The disturbance environment is simulated for a sinusoidal pitch angle of $\pm 1.5^\circ$ and a

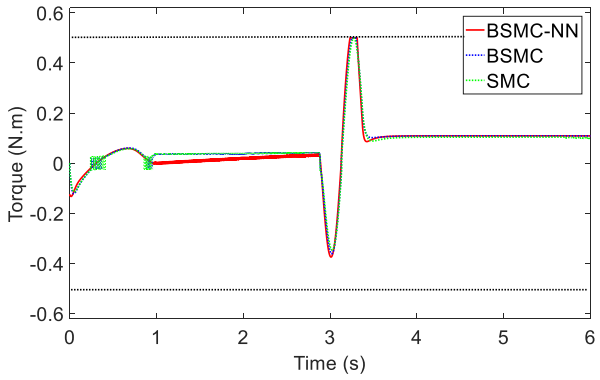

FIGURE 8. Case 2: Motor torque.

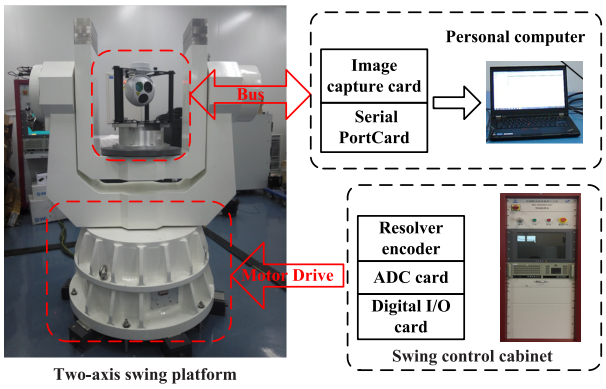

FIGURE 9. Experiments System configuration.

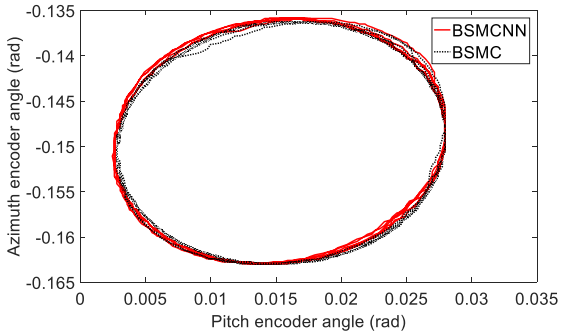

FIGURE 10. Pitch and azimuth encoder angle curve.

frequency of 1Hz. The sampling frequency of the signal is 125Hz, and the gyro signal and encoder values are stored and displayed to the host computer through the serial bus. The host computer can also display a scene picture captured by the visible light camera in real time.

The control subroutine with 1KHz sampling rate first executes the tracking target command, and locks a stationary target at a focal length of 129mm of the visible light camera via the BSMC-NN and BSMC control algorithms. Then, the swing platform system movement simulates pitch and azimuth external vibration at same time. In addition, the angle positions and angle velocity are recorded from the resolver encoder sensor and gyro value. Fig. 10 shows a picture with the pitch axis encoder value as the x-axis and the azimuth

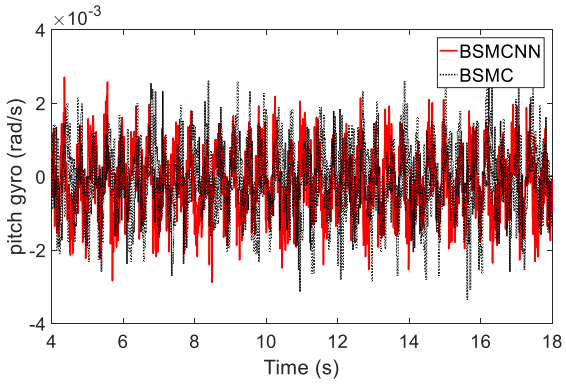

FIGURE 11. Pitch gyro curve.

TABLE 2. Performance comparison of both different algorithms.

Pitch gimbal response	Parameter	BSMC-NN	BSMC
Tracking angle error (mrad)	Absolute maximum	0.045	0.073
	RMS	0.021	0.034
Angle velocity (mrad/s)	Absolute maximum	2.8	3.3
	RMS	0.092	0.096

axis encoder value as the y-axis. Fig.10 shows that the red curve using the BSMC-NN method is smoother than the black dotted line with BSMC control.

From the intercepted 4 sec to 18 sec of gyro data in Fig.11, the value of proposed control method approaches a stable range of −2.8 mrad/sand 2.7 mrad/s. The angle velocity peak to peak of the BSMC control strategy is between about −3.3mrad/s and 2.8 mrad/s. The tracking and stability performance comparison of both two control algorithms are shown in Table 2. Although both control strategies have a similar peak to peak value, the RMS angle velocity of the proposed control method is 0.092, which is smaller than that of the BSMC control.

V. CONCLUSIONS

This paper presents a mathematical model of a two-axis gimbal system that considers the most important disturbance sources, such as parametric uncertainties, dynamic friction and input saturation. A backstepping sliding mode controller combined with adaptive neural networks approach (BSMC-NN) is proposed for the ISP system. In particular, an auxiliary design function is explicitly considered for the actuator saturation problem. Uncertain nonlinear disturbances have been approximated by RBFNN using defined functions. The updating law for the on-line learning of the RBFNN and the stability of the closed loop system are derived using the Lyapunov theorem. For the numerical simulations, the mass imbalance and the base rotations disturbances under both two typical ground vehicle cases are considered to validate the performance of this controller. Comparative simulations and experiments both show that the

BSMC-NN approach can realize the desired attitude control and the high-precision stabilization performance.

REFERENCES

[1] D. Anderson, "Evolutionary algorithms in airborne surveillance systems: Image enhancement via optimal sightline control," *Inst. Mech. Eng., G, J. Aerosp. Eng.*, vol. 225, no. 10, pp. 1097–1108, 2011.
[2] K. Jędrasiak, D. Bereska, and A. Nawrat, "The prototype of gyro-stabilized UAV gimbal for day-night surveillance," in *Advanced Technologies for Intelligent Systems of National Border Security*. Berlin, Germany: Springer, 2013, pp. 107–115.
[3] H. X. Jiang, Z. S. Ding, and Y. Y. Wang, "Inertial stabilization and attitude tracking in the geographic coordinate system of the large platform," *Navigat. Control*, vol. 16, no. 3, pp. 12–17, 2017.
[4] X. Zhou, Y. Jia, Q. Zhao, and R. Yu, "Experimental validation of a compound control scheme for a two-axis inertially stabilized platform with multi-sensors in an unmanned helicopter-based airborne power line inspection system," *Sensors*, vol. 16, no. 3, p. 366, 2016.
[5] G. Fursht and M. Idan, "Experimental evaluation of sliding-mode controller for seeker-head line-of-sight stabilization," *J. Guid., Control, Dyn.*, vol. 39, no. 10, pp. 1–5, 2016.
[6] Y. Xia, L. Dai, M. Fu, C. Li, and C. Wang, "Application of active disturbance rejection control in tank gun control system," *J. Franklin Inst.*, vol. 351, no. 4, pp. 2299–2314, 2014.
[7] M. Abdo, A. R. Vali, A. Toloei, and M. R. Arvan, "Research on the cross-coupling of a two axes gimbal system with dynamic unbalance," *Int. J. Adv. Robot. Syst.*, vol. 10, no. 10, p. 357, 2013.
[8] R. Jia, V. K. Nandikolla, G. Haggart, C. Volk, and D. Tazartes, "System performance of an inertially stabilized gimbal platform with friction, resonance, and vibration effects," *J. Nonlinear Dyn.*, vol. 2017, Mar. 2017, Art. no. 6594861.
[9] A. Safa and R. Y. Abdolmalaki, "Robust output feedback tracking control for inertially stabilized platforms with matched and unmatched uncertainties," *IEEE Trans. Control Syst. Technol.*, vol. 27, no. 1, pp. 118–131, Jan. 2017.
[10] M. S. Sofla, M. Zareinejad, M. Parsa, and H. Sheibani, "Integral based sliding mode stabilizing a camera platform using Kalman filter attitude estimation," *Mechatronics*, vol. 44, pp. 42–51, Jun. 2017.
[11] H. X. Jiang, W. Zhang, and X. D. Lu, "Design and implementation of stabilization platform control system for gravity measurement," *Navigat. Control*, vol. 15, no. 6, pp. 51–56, 2016.
[12] K.-J. Seong, H.-G. Kang, B.-Y. Yeo, and H.-P. Lee, "The stabilization loop design for a two-axis gimbal system using LQG/LTR controller," in *Proc. SICE-ICASE Int. Joint Conf.*, 2006, pp. 755–759.
[13] K. Deng, S. Cong, D. Kong, and H. Shen, "Discrete-time direct model reference adaptive control application in a high-precision inertially stabilized platform," *IEEE Trans. Ind. Electron.*, vol. 66, no. 1, pp. 358–367, Jan. 2018.
[14] M. Rezác and Z. Hurák, "Structured MIMO H_∞ design for dual-stage inertial stabilization: Case study for HIFOO and Hinfstruct solvers," *Mechatronics*, vol. 23, no. 8, pp. 1084–1093, 2013.
[15] M. Zhang, H. Liu, H. Zhang, and X. Miao, "A hybrid control strategy for the optoelectronic stabilized platform of a seeker," *Optik*, vol. 181, pp. 1000–1012, Mar. 2019.
[16] F. Liu, H. Wang, Q. Shi, H. Wang, M. Zhang, and H. Zhao, "Comparison of an ANFIS and fuzzy PID control model for performance in a two-axis inertial stabilized platform," *IEEE Access*, vol. 5, pp. 12951–12962, 2017.
[17] C. Hu, Z. Wang, Y. Qin, Y. Huang, J. Wang, and R. Wang, "Lane keeping control of autonomous vehicles with prescribed performance considering the rollover prevention and input saturation," *IEEE Trans. Intell. Transp. Syst.*, to be published. doi: 10.1109/TITS.2019.2924937.
[18] Y. Qin, F. Zhao, Z. Wang, L. Gu, and M. Dong, "Comprehensive analysis for influence of controllable damper time delay on semi-active suspension control strategies," *J. Vib. Acoust.*, vol. 139, Mar. 2017, Art. no. 031006.
[19] Y. Qin, Z. Wang, C. Xiang, E. Hashemi, A. Khajepour, and Y. Huang, "Speed independent road classification strategy based on vehicle response: Theory and experimental validation," *Mech. Syst. Signal Process.*, vol. 117, pp. 653–666, Feb. 2019. doi: 10.1016/j.ymssp.2018.07.035.
[20] O. Hasturk, A. M. Erkmen, and I. Erkmen, "Proxy-based sliding mode stabilization of a two-axis gimbaled platform," *Target*, vol. 3, no. 4, pp. 1–7, 2011.
[21] S. B. Kim, S. H. Kim, and Y. K. Kwak, "Robust control for a two-axis gimbaled sensor system with multivariable feedback systems," *IET Control Theory Appl.*, vol. 4, no. 4, pp. 539–551, 2010.
[22] B. Ahi and A. Nobakhti, "Hardware implementation of an ADRC controller on a gimbal mechanism," *IEEE Trans. Control Syst. Technol.*, vol. 26, no. 6, pp. 2268–2275, Nov. 2018.
[23] M. M. Abdo, A. R. Vali, A. R. Toloei, and M. R. Arvan, "Stabilization loop of a two axes gimbal system using self-tuning PID type fuzzy controller," *ISA Trans.*, vol. 53, no. 2, pp. 591–602, Mar. 2014.
[24] M. Chen, B. Jiang, J. Zou, and X. Feng, "Robust adaptive tracking control of the underwater robot with input nonlinearity using neural networks," *Int. J. Comput. Intell. Syst.*, vol. 3, no. 5, pp. 646–655, 2010.
[25] G.-X. Wen, C. L. P. Chen, Y.-J. Liu, and Z. Liu, "Neural-network-based adaptive leader-following consensus control for second-order nonlinear multi-agent systems," *IET Control Theory Appl.*, vol. 9, no. 13, pp. 1927–1934, Aug. 2015.
[26] C. Hu, Z. Wang, H. Taghavifar, J. Na, Y. Qin, J. Guo, and C. Wei, "MME-EKF-based path-tracking control of autonomous vehicles considering input saturation," *IEEE Trans. Veh. Technol.*, vol. 68, no. 6, pp. 5246–5259, Jun. 2019. doi: 10.1109/TVT.2019.2907696.
[27] Z. Wang, Y. Qin, C. Hu, M. Dong, and F. Li, "Fuzzy observer-based prescribed performance control of vehicle roll behavior via controllable damper," *IEEE Access*, vol. 7, pp. 19471–19487, 2019.
[28] J. Fang, R. Yin, and X. Lei, "An adaptive decoupling control for three-axis gyro stabilized platform based on neural networks," *Mechatronics*, vol. 27, pp. 38–46, Apr. 2015.
[29] S. Gayaka, L. Lu, and B. Yao, "Global stabilization of a chain of integrators with input saturation and disturbances: A new approach," *Automatica*, vol. 48, no. 7, pp. 1389–1396, 2012.
[30] B. Zhou, J. Lam, and G.-R. Duan, "An ARE approach to semi-global stabilization of discrete-time descriptor linear systems with input saturation," *Syst. Control Lett.*, vol. 58, no. 8, pp. 609–616, 2009.
[31] M. Chen, B. Ren, Q. Wu, and C. Jiang, "Anti-disturbance control of hypersonic flight vehicles with input saturation using disturbance observer," *Sci. China Inf. Sci.*, vol. 58, no. 7, pp. 1–12, 2015.
[32] J. Song, D. Zhou, and G. Sun, "Adaptive robust control for mirror-stabilized platform with input saturation," *J. Dyn. Syst., Meas., Control*, vol. 40, no. 9, 2018, Art. no. 091014.
[33] Y. Hong and B. Yao, "A globally stable high-performance adaptive robust control algorithm with input saturation for precision motion control of linear motor drive systems," *IEEE/ASME Trans. Mechatronics*, vol. 12, no. 2, pp. 198–207, Apr. 2007.
[34] C. Pukdeboon, "Anti-disturbance inverse optimal control for spacecraft position and attitude maneuvers with input saturation," *Adv. Mech. Eng.*, vol. 8, no. 5, pp. 1–14, 2016.
[35] Y.-Y. Min and Y.-G. Liu, "Barbalat lemma and its application in analysis of system stability," *J. Shandong Univ. (Eng. Sci.)*, vol. 37, no. 1, pp. 51–55, 2007.
[36] Y. Qin, Z. Wang, C. Xiang, M. Dong, C. Hu, and R. Wang, "A novel global sensitivity analysis on the observation accuracy of the coupled vehicle model," *Vehicle Syst. Dyn.*, 2019, doi: 10.1080/00423114.2018.1517219.
[37] F. Zhao, S. S. Ge, F. Tu, Y. Qin, and M. Dong, "Adaptive neural network control for active suspension system with actuator saturation," *IET Control Theory Appl.*, vol. 10, no. 14, pp. 1696–1705, Sep. 2016.

ZHUSHUN DING received the master's degree in mechanical engineering from North China Electric Power University, China, in 2001. He is currently pursuing the Ph.D. degree with the National University of Defense Technology, Changsha, China. Since 2010, he has been the Director of the Gyroscope-Stabilized Laboratory, Beijing Institute of Aerospace Control Devices. His research interests include mechanical system dynamics, damper design, and modeling gyroscope-stabilized platform.

FENG ZHAO received the Ph.D. degree in aeronautical and astronautical science and technology from the Beijing Institute of Technology, China, in 2016. From 2014 to 2015, he was a Visiting Scholar with the National University of Singapore. Since 2016, he has been with the Beijing Institute of Aerospace Control Devices. His research interests include mechanical dynamics, nonlinear state estimation, and modeling gyroscope-stabilized platform.

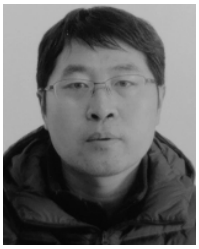

YUEDONG LANG received the Ph.D. degree in mechanical engineering from the Harbin Institute of Technology, China, in 2010. Since 2010, he has been with the Beijing Institute of Aerospace Control Devices. His research interests include mechanical dynamics, virtual reality, modeling of robot, and photoelectric pod design.

ZHE JIANG received the master's degree in electrical engineering from the Narvik University College, Norway, in 2012. Since 2012, he has been with the Beijing Institute of Aerospace Control Devices. His research interests include controllable suspension systems, modeling of robot, and photoelectric pod control.

JIAJING ZHU received the master's degree in Science from The University of Sheffield, in 2015. Since 2015, she has been with the Research and Development Management Department, Beijing Institute of Aerospace Control Devices. Her main research interests include automatic control and circuit design.